JOURNAL PRE-PROOF

This is an early version of the article, published prior to copyediting, typesetting, and editorial correction. The manuscript has been accepted for publication and is now available online to ensure early dissemination, author visibility, and citation tracking prior to the formal issue publication.

It has not undergone final language verification, formatting, or technical editing by the journal's editorial team. Content is subject to change in the final Version of Record.

To differentiate this version, it is marked as "PRE-PROOF PUBLICATION" and should be cited with the provided DOI. A visible watermark on each page indicates its preliminary status.

The final version will appear in a regular issue of *Archives of Acoustics*, with final metadata, layout, and pagination.

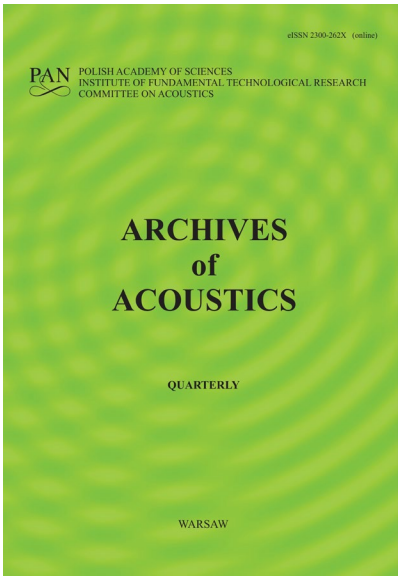

Title: An Improved Dynamic Time Warping Algorithm for Active Sonar Signal Matching

Author(s): Tongjing Sun, Hunyuan Wang, Lei Chen, Haoran Xu

DOI: https://doi.org/10.24423/archacoust.2026.4295

Journal: *Archives of Acoustics*

ISSN: 0137-5075, e-ISSN: 2300-262X

Publication status: In press

Received: 2025-08-07

Revised: 2025-11-27

Accepted: 2025-12-10

Published pre-proof: 2026-01-16

Please cite this article as:

Sun T., Wang H., Chen L., Xu H. (2026), An Improved Dynamic Time Warping Algorithm for Active Sonar Signal Matching, *Archives of Acoustics*, https://doi.org/10.24423/archacoust.2026.4295

An Improved Dynamic Time Warping Algorithm for Active Sonar Signal Matching

Tongjing Sun*, Hunyuan Wang, Lei Chen, Haoran Xu

Department of Automation, Hangzhou Dianzi University, Hangzhou, China
*Corresponding Author: stj@hdu.edu.cn

Active sonar signal matching is a critical technique for measuring inter-signal similarity and enhancing target detection and classification performance. However, in complex underwater environments, noise, reverberation, and prolonged signal durations often degrade matching accuracy and computational efficiency. To address these challenges, this paper proposes an Adaptive Extremum-aligned Boundary-constrained Dynamic Time Warping (AEB-DTW) algorithm, based on the classical Dynamic Time Warping (DTW) framework. The algorithm extracts significant extrema from signal envelopes to suppress noise and reverberation while capturing salient features. By integrating the position and amplitude of extrema, an adaptive weighted matching strategy is introduced to enhance feature discrimination. In addition, spline fitting is applied to the residuals of the extremum matching path to dynamically generate upper and lower boundary constraints, thus restricting DTW computation to a meaningful region and achieving a balance between accuracy and efficiency. Experiments using lake-trial active sonar data under signal-to-reverberation ratios (SRRs) from 0 dB to 30 dB show that AEB-DTW outperforms ED, DTW, and its variants in matching accuracy, robustness, and angular resolution, while significantly improving computational efficiency, particularly for long-duration signals.

Keywords: Active sonar signal matching; Dynamic Time Warping (DTW); Time series similarity; Adaptive boundary constraints.

1 Introduction

Active sonar signals, as a typical type of time-series data, play a crucial role in underwater navigation, target detection, and marine resource exploration (Bian *et al*., 2024; Zhang *et al*., 2023; Zhu *et al*., 2025). In complex marine environments, efficiently and accurately measuring

the similarity between signals is a fundamental basis for supporting applications such as target detection, localization, feature extraction, and classification using active sonar (Sun *et al*., 2024; Dau *et al*., 2018). It also has a profound impact on improving the processing efficiency and recognition performance of subsequent tasks (Silva *et al*., 2018).

Dynamic Time Warping (DTW) is a widely used algorithm for time-series alignment that addresses limitations of traditional Euclidean distance (ED) metrics by allowing nonlinear temporal warping (Wang *et al*., 2022; Chen *et al*., 2017). DTW effectively handles sequences of differing lengths, temporal shifts, and amplitude variations, enabling robust and precise matching (Li, Guo, 2013). Consequently, it has attracted extensive research attention globally.

To improve computational efficiency, methods such as LB_Yi, LB_Kim, and LB_Keogh have been proposed by Yi *et al*. (1998), Kim *et al*. (2001), and Keogh *et al*. (2005), respectively. These methods define lower-bound constraints on sequence distances to exclude dissimilar sequences and reduce the search space for matching. Salvador and Chan (2007) introduced the Fast-DTW algorithm, which reduces computational cost by projecting sequences into low-dimensional spaces to approximate the warping path. Lahreche and Boucheham (2021) developed LEDTW, which significantly reduces complexity by performing DTW only on local extrema. Tang and Gao (2023) proposed EWDTW, incorporating adaptive weighting strategies based on local extrema to enhance both efficiency and classification accuracy. Sakoe and Chiba (1978) introduced the Sakoe-Chiba band, which constrains the warping path's search area to reduce matrix computations.

For improving alignment accuracy, Jeong *et al.* (2011) and Li (2021) proposed WDTW and TWDTW, which adjust feature weights to enhance alignment precision. Keogh and Pazzani (2001) introduced DDTW, which focuses on the trend of sequence variation by incorporating first-order derivatives to avoid misalignments. Li *et al*. (2020) proposed ACDTW, which dynamically adjusts the warping window to better match local features. Zhao and Itti

(2018) proposed ShapeDTW, which uses local extremum structures to enhance the ability to identify complex shapes. Hong *et al*. (2020) proposed SSDTW, which combines sparse representation with spatial structural constraints for efficient high-dimensional sequence alignment.

Despite these developments, existing DTW variants still struggle to balance alignment accuracy and computational efficiency for active sonar echoes. In complex underwater environments, strong reverberation and noise distort signal envelopes, causing unstable similarity estimation, while fixed or manually tuned warping constraints fail to adapt to variable signal durations. Therefore, the core technical problem addressed in this work is achieving robust and efficient similarity matching for active sonar signals under low signal-to-reverberation ratio (SRR) conditions while preserving key structural features.

To solve this problem, this study proposes an Adaptive Extremum-aligned Boundary-constrained Dynamic Time Warping (AEB-DTW) algorithm. The method extracts significant extrema to suppress noise and highlight salient envelope structures, introduces adaptive weighting to enhance feature discrimination, and constructs dynamic boundary constraints to reduce computation while maintaining alignment precision. The main contributions are developing a structure-aware matching framework, achieving a robustness–efficiency balance, and validating its effectiveness through comprehensive lake-trial experiments against ED, DTW, and its variants.

2 Dynamic Time Warping (DTW) Algorithm

The core objective of the DTW algorithm is to find an optimal alignment path that minimizes the overall distance between two sequences. Let the envelope features of two one-dimensional active sonar signals be $\mathbf{X}=\{x_1,\cdots,x_i,\cdots,x_m\}$ and $\mathbf{Y}=\{y_1,\cdots,y_i,\cdots,y_n\}$, with lengths *m* and *n*, respectively, as shown in Fig. 1(a).

To implement this optimal alignment, we turn to the DTW matching process, which is illustrated in Fig. 1(b): sequences **X** and **Y** are mapped to the horizontal and vertical axes of a two-dimensional grid to construct a distance matrix. Using the principle of minimum cumulative distance, the shortest path from the bottom-left corner to the top-right corner is found, representing the optimal nonlinear alignment between the two sequences. Fig. 1(c) shows the pointwise correspondence along the optimal warping path.

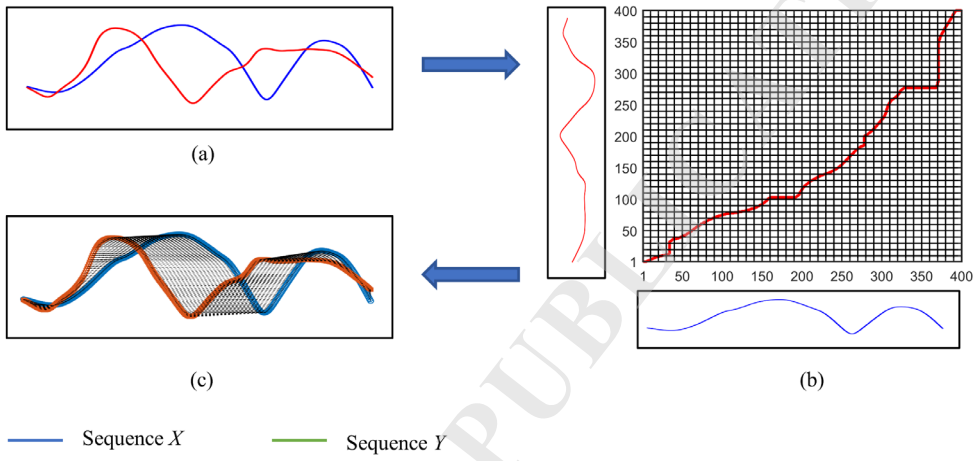

Fig. 1. DTW Alignment Effect and Warping Path.

To compute the DTW distance between sequences **X** and **Y**, we first define the point-wise distance function between elements x_i and y_j:

$$d(i,j) = \left\| x_i - y_j \right\|_\beta , \tag{1}$$

where $\beta \in \mathbb{R}^+$, and $\beta = 2$ corresponds to the Euclidean distance. To compute the DTW distance between sequences **X** and **Y**, an optimal warping path must be identified. Let this optimal path be denoted as:

$$\mathbf{W} = \{(i_1, j_1), (i_2, j_2), \cdots, , (i_k, j_k), (i_K, j_K)\}, \tag{2}$$

where K is the length of the warping path, and each (i_k, j_k) represents a matched pair of indices from sequences **X** and **Y**, respectively. The warping path **W** is an ordered set of index pairs that aligns the two sequences in a nonlinear manner. Its formal constraints and cost computation are described as follows.

1) Boundary condition: $(i_1, j_1) = (1,1)$, and $(i_K, j_K) = (m, n)$.

2) Monotonicity: $i_{k+1} \geq i_k$, $j_{k+1} \geq j_k$.

3) Continuity: $(i_{k+1} - i_k, j_{k+1} - j_k) \in \{(1,0),(0,1),(1,1)\}$.

Under these constraints, the DTW distance is calculated as:

$$DTW(\mathbf{X}, \mathbf{Y}) = \min_{\mathbf{W}} \left\{ \sum_{k=1}^{K} d(i, j) \right\}. \tag{3}$$

To solve this, a cumulative cost matrix $\mathbf{D}$ is constructed recursively as:

$$D(i, j) = d(i, j) + \min\{D(i-1, j), D(i, j-1), D(i-1, j-1)\}, \tag{4}$$

where $i = 1, 2, \cdots, m$, $j = 1, 2, \cdots, n$. The initial conditions are set as $D(0,0) = 0$, and $D(i,0) = D(0, j) = \infty$. Equation (4) indicates that the cumulative distance at a given point equals the sum of the current pointwise distance and the minimum cumulative distance from its neighboring positions. $D(m, n)$ denotes the DTW distance between sequences **X** and **Y**, and the computational complexity of the algorithm is *O(m*n)*.

3 The AEB-DTW Algorithm

The core idea of the AEB-DTW algorithm is to adaptively extract significant extrema from active sonar signal envelopes in order to capture key structural features. A weighted matching model is constructed using amplitude and phase differences to enhance the discrimination ability of extrema alignment. Based on the weighted matching results, a dynamic upper and lower boundary constraint is constructed to restrict the DTW search region, thereby enhancing both efficiency and robustness.

Fig. 2 illustrates the processing flow of AEB-DTW. The signal envelope is first extracted to highlight major structures and suppress noise (Fig. 2(a)). Then, significant extrema are

adaptively identified to form a reduced feature sequence (Fig. 2(b)). These extrema are assigned adaptive weights according to their position and amplitude to guide the warping path (Fig. 2(c)). Finally, boundary constraints are constructed from the residuals between the matched extrema path and the smoothed trend line (Fig. 2(d)).

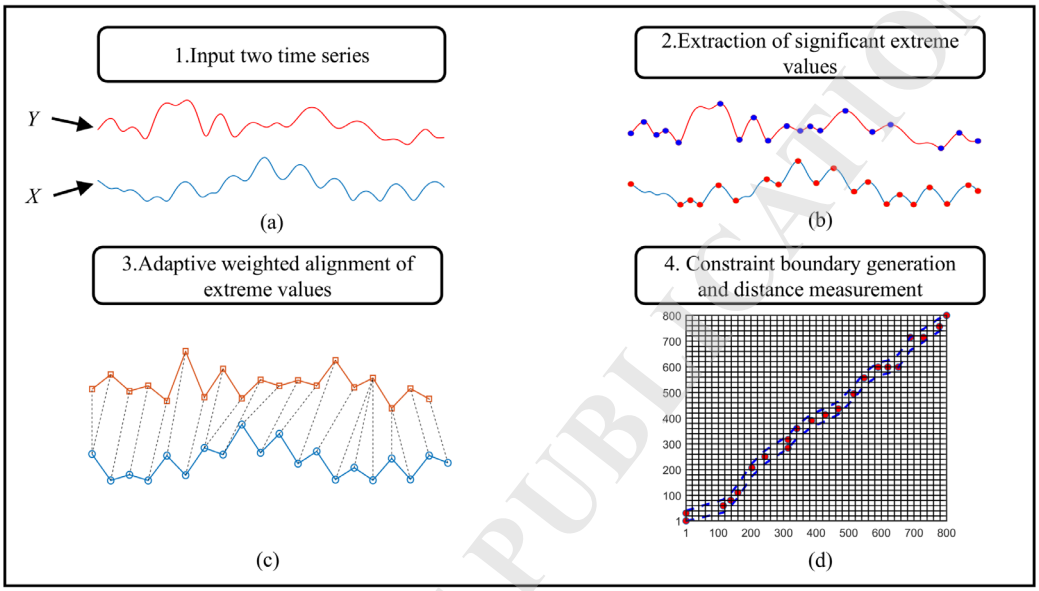

Fig. 2. Execution Flow of the AEB-DTW Algorithm.

3.1 Extraction of Significant Extrema

To extract structurally meaningful local extrema from active sonar signal envelopes, we adopt a prominence-based adaptive detection method. For a given sequence $\mathbf{X}=\{x_1,\cdots,x_k,\cdots,x_m\}$, each point $x_k\,(k=2,3,\cdots,m-1)$ is identified as a local maximum if $x_{k-1}<x_k>x_{k+1}$, or a local minimum if $x_{k-1}>x_k<x_{k+1}$.

To determine whether a local extremum is significant, a dynamic threshold is introduced based on the statistical characteristics of the signal. Let μ, $x_{\min}$ and $x_{\max}$ denote the mean, minimum, and maximum values of $\mathbf{X}$, respectively. A scaling factor γ is defined as:

$$\gamma=\frac{\mu-x_{\min}}{x_{\max}-x_{\min}}. \tag{5}$$

Based on this, the prominence threshold δ is computed as:

$$\delta = \gamma \cdot \mathrm{MAD}(\mathbf{X}), \tag{6}$$

where MAD(**X**) is the mean absolute deviation, which measures average signal fluctuation and is robust to outliers. Local extrema are retained only if their prominence exceeds δ, effectively suppressing noise-induced oscillations and weak fluctuations.

The prominence of a local extremum quantifies how much it stands out from its surroundings. For a maximum, it is defined as the vertical distance between the peak and the lowest point on either side before reaching a higher peak. For a minimum, it is the distance between the trough and the highest point between it and a deeper trough.

Let $\mathbf{X}_\mathbf{E} = \{(p_i, a_i)\}_{i=1}^{m'}$ and $\mathbf{Y}_\mathbf{E} = \{(q_j, b_j)\}_{j=1}^{n'}$ denote the sequences of significant extrema extracted from **X** and **Y**, respectively, where p_i and q_j are the positions (indices) of the *i*-th and *j*-th significant extreme points, and a_i and b_j are the corresponding amplitudes. For two sequences of lengths *m* and *n*, the numbers of significant extrema extracted are *m′* and *n′*, respectively, where $m' \leq m$ and $n' \leq n$. As illustrated in Fig. 3, peaks and troughs correspond to local maxima and minima of the signal. Only extrema exceeding the adaptive saliency threshold are retained, while non-significant extrema caused by noise are excluded. The start and end points are added to the extrema sets $\mathbf{X}_\mathbf{E}$ and $\mathbf{Y}_\mathbf{E}$ to preserve boundary characteristics. Although some local extrema are not detected (indicated by arrows in Fig. 3), these omissions do not affect the extraction of essential structural features, ensuring algorithmic correctness and stability while enabling dimensionality reduction.

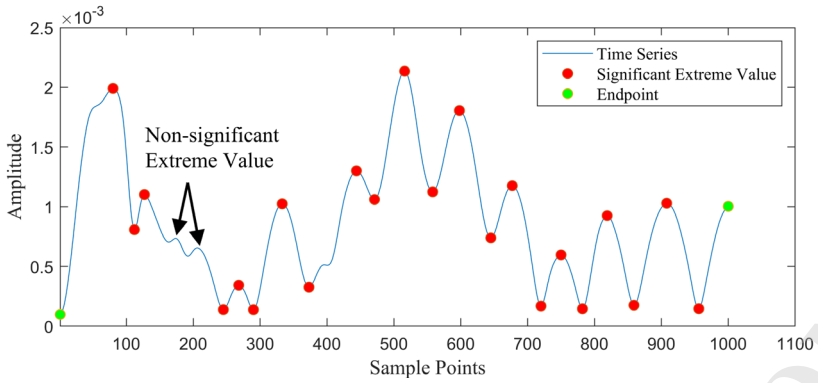

Fig. 3. Extraction Process of Significant Local Extrema.

3.2 Adaptive Weighted Alignment of Significant Extrema

After extracting significant extrema from both sequences, the next step is to establish reliable correspondences. As key structural features, the accurate alignment of these extrema provides a foundation for reducing the search space and enhancing the robustness of similarity matching. To this end, a weighted alignment strategy is proposed, which jointly models the positional and amplitude attributes of each extremum to characterize structural correspondences more precisely. Significant extrema are regarded as fundamental matching units, and their fused features are used to construct weighted correspondences. The resulting position mappings serve as the structural basis for generating boundary constraints, as detailed below.

$$D_E(i,j) = \omega_b \cdot |a_i - b_j| + \omega_a \cdot |p_i - q_j| + \min \begin{cases} D_E(i-1,j) \\ D_E(i,j-1) \\ D_E(i-1,j-1) \end{cases}, \tag{7}$$

where $\omega_a = \lambda/(1+r)$ and $\omega_b = 1-\omega_a$ represent the weighting coefficients for positional and amplitude differences, respectively. Here, $\boldsymbol{\lambda} = 0.6$ is a weighting constant used to establish a stable numerical relationship between the two components. The ratio $\mathbf{r}$ reflects the relative difference between amplitude and position, and is computed as follows:

$$\mathbf{r} = \frac{\Delta p_x + \Delta p_y}{\Delta a_x + \Delta a_y}, \tag{8}$$

where Δp_x , Δa_x , Δp_y , and Δa_y respectively represent the position average difference change rate and the amplitude average difference change rate of the extreme value sequences $\mathbf{X_E}$ and $\mathbf{Y_E}$. The average change rates of the position and amplitude of the significant extreme value points are defined as follows:

$$\Delta p = \frac{1}{N-1}\sum_{i=1}^{N-1}\left|\frac{pos(i+1)-pos(i)}{L}\right|, \tag{9}$$

$$\Delta a = \frac{1}{N-1}\sum_{i=1}^{N-1}\left|value(i+1)-value(i)\right|, \tag{10}$$

where $L=\lfloor (m+n)/2 \rfloor$ is the normalized length of the time axis, N represents the number of significant extreme value points, $pos(i)$ and $value(i)$ represent the position and amplitude of the *i*-th significant extreme value point. For $\mathbf{X_E}$, $N=m'$, $pos(i)=p_i$, $value(i)=a_i$. Similarly, for $\mathbf{Y_E}$, $N=n'$, $pos(i)=q_i$, $value(i)=b_i$.

Through the above-mentioned distance measurement, an optimal warping path will be obtained. Let the extremum alignment path be denoted by $\mathbf{W_E}=\{(p_k,q_k)\}_{k=1}^{T}$ where T is the number of aligned pairs in the path; $p_k \in P_X$ (with $P_X=\{p_1,p_2,\cdots,p_{m'}\}$ being the position set of significant extrema in $\mathbf{X_E}$) and $q_k \in P_Y$ (with $P_Y=\{q_1,q_2,\cdots,q_{n'}\}$ being the position set of significant extrema in $\mathbf{Y_E}$) are the temporal positions of significant extrema in $\mathbf{X_E}$ and $\mathbf{Y_E}$, respectively. The path $\mathbf{W_E}$ satisfies the standard DTW constraints and is derived by minimizing the weighted distance metric, thus establishing the structural correspondence between the two extremum sequences.

3.3 Dynamic Time Warping with Boundary Constraints

To improve efficiency and robustness, AEB-DTW incorporates boundary constraints using

matched significant extrema as anchors. Weighted extrema alignments are treated as 2D points, to which a smoothing spline is fitted; residuals define discrete upper and lower boundaries, which are linearly interpolated over the reference sequence. This confines the DTW path to a meaningful region, reducing computational load and misalignments. The extrema path captures global trends, while the residual-based envelope reflects local variations, enabling semantically meaningful alignment under noise. As shown in Fig. 4, AEB-DTW produces fewer spurious matches than standard DTW.

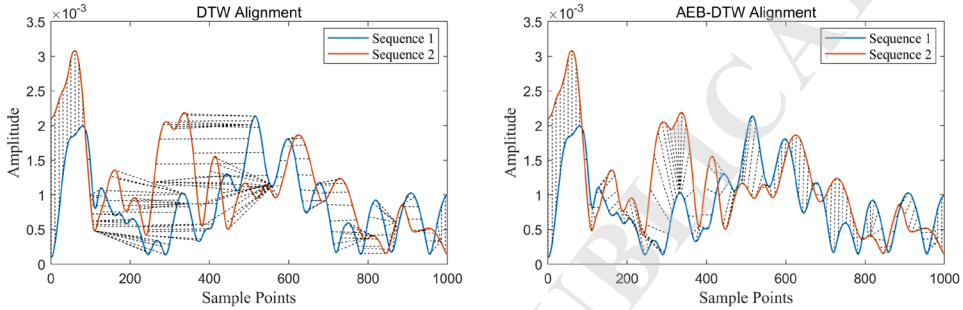

Fig. 4. Comparison of Alignment Effects Between DTW and AEB-DTW.

The construction process of the upper and lower boundaries is as follows: First, the significant extremum matching path $\mathbf{W}_{\mathbf{E}}$ is treated as discrete points in the two-dimensional coordinate space. These points, shown as the red dots in Fig. 5(a), have coordinates (p_k, q_k) that denote the positions of significant extrema in sequences **X** and **Y**, respectively. Then, a smoothing spline is applied to these points to obtain the fitted curve $f(k)$. This curve captures the positional alignment trend between the two sequences and predicts the corresponding position q_k in **Y** for each p_k in **X**.

Subsequently, the absolute residuals between the actual matched points and the fitted curve are calculated, and the 95th percentile of these residuals, denoted as res_{95}, is used as the width of the constraint band. Using this width, discrete upper and lower boundary points are constructed, which are then extended to the full index range of the reference sequence via linear

interpolation. This results in the complete boundary functions LB and UB, as illustrated in Fig. 5(b).

The construction of the discrete upper and lower boundaries is as follows:

$$UB(p_k) = \min\left(m, \max\left(q_k, f(p_k) + res_{95}\right)\right), \tag{11}$$

$$LB(p_k) = \max\left(1, \min\left(q_k, f(p_k) - res_{95}\right)\right). \tag{12}$$

At this stage, the upper and lower boundary functions are only defined at the discrete points p_k and have not yet covered the entire range of the reference sequence. To address this, linear interpolation is applied to the sets of boundary points $\left(p_k, LB(p_k)\right)$ and $\left(p_k, UB(p_k)\right)$, respectively, resulting in continuous functions that are fully defined over the index range of the reference sequence. The interpolated functions ensure that at each time index *i*, a valid upper and lower constraint boundary is provided. Accordingly, the DTW path search region is finally constrained within the following area:

$$B = \left\{(i, j) \middle| LB(i) \le j \le UB(i), i \in [1, m]\right\}. \tag{13}$$

Within this region, the DTW alignment path **P** must satisfy the standard DTW conditions of boundary, monotonicity, and continuity. The AEB-DTW distance is finally computed as:

$$AEB - DTW(\mathbf{X}, \mathbf{Y}) = \min_{\mathbf{P} \subseteq B} \sum_{(i,j) \in \mathbf{P}} d\left(x_i, y_j\right), \tag{14}$$

where $d\left(x_i, y_j\right)$ is the local distance function between points x_i and y_j, as defined in standard DTW. This boundary-constrained DTW framework not only significantly reduces computational overhead, but also improves alignment reliability by preventing implausible matches.

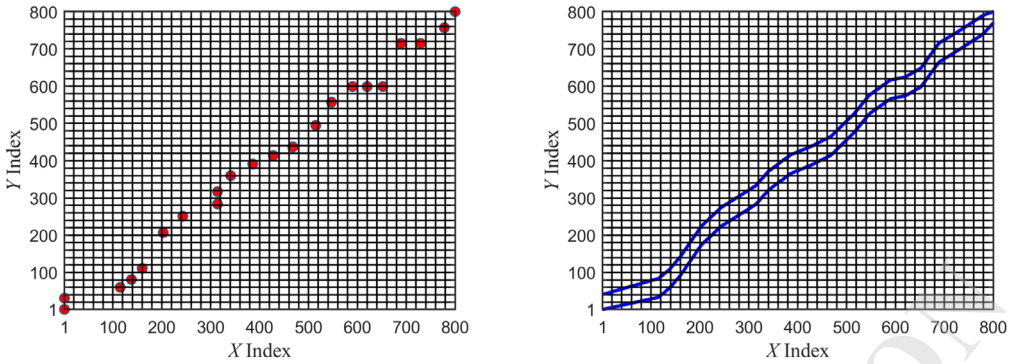

(a) Extreme Position Alignment Path (b) Upper and Lower Boundary Constraints

Fig. 5. Formation Process of the Boundary Constraint.

4 Performance Validation Based on Measured Data

4.1 Overview of Measured Data

The lake trial was conducted on October 25, 2024, at the Moganshan Reservoir in Deqing County, Huzhou City, Zhejiang Province. The test target was a submarine-like model. The transmitted signal was a linear frequency modulated (LFM) pulse with a frequency range of 10 kHz to 20 kHz, a pulse width of 4 ms, and a sampling rate of 500 kHz.

As shown in Fig. 6(a), the experiment employed a bistatic sonar configuration, with the transmitter and hydrophone separated by 7 m, and the target located 14 m from the hydrophone, all positioned in the same horizontal plane at a water depth of approximately 5 m. Fig. 6(b) shows a photograph of the experimental data acquisition system. The dry-end electronic equipment on the transmitting side includes a power amplifier, a signal source, and an oscilloscope, while that on the receiving side includes a data acquisition unit and a computer. The transmitting device is a transmitting transducer, and the receiving device is a receiving hydrophone.

The target was mounted on a servo-driven platform rotating uniformly counterclockwise. The platform completed a 180° turn in about 3 minutes; with a pulse repetition interval of 0.6

s, this corresponds to a rotation speed of approximately 1°/s and an azimuth step of about 0.6° per transmission. Consequently, the 300 recorded echoes form a full 180° azimuth scan of the target, with each echo corresponding to a fixed angular increment relative to the transmitter–receiver baseline.

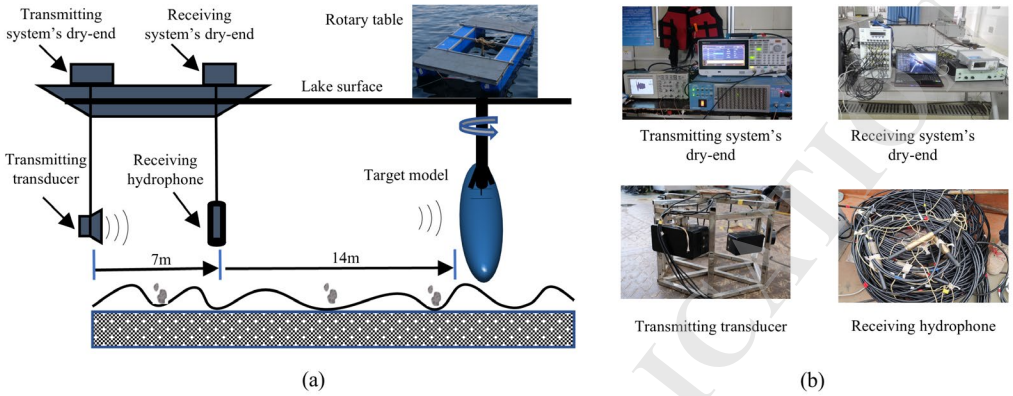

Fig. 6. Experimental Setup and Equipment Configuration.

The signal processing procedure is illustrated in Fig. 7(a). The Original Signal refers to the segment extracted from the raw measurements that contains the target echo. Sparse reconstruction is first applied to this segment to enhance signal quality. The envelope of the reconstructed signal is then obtained to characterize overall amplitude variation and improve stability, providing a reliable input for subsequent matching. Fig. 7(b) shows the matched-filtering results of reconstructed signals from different bearing angles. The matched-filter responses reveal the target's attitude variations with bearing, thereby supporting the rationality of the subsequent matching results.

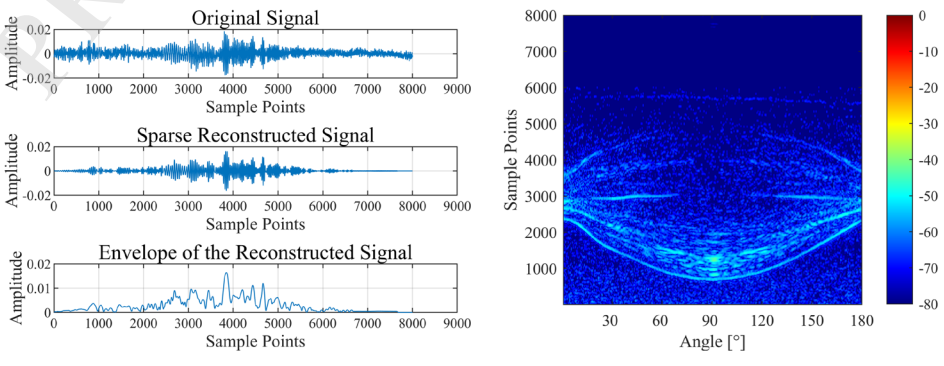

Fig. 7. Signal Processing Flow.

4.2 Validation of Matching Accuracy and Anti-Interference Capability

To evaluate the robustness of the algorithm under different interference conditions, echo signals with specified SRRs were synthesized from sparsely reconstructed lake-trial echoes. Each measured echo was first processed by the sparse reconstruction procedure described in Section 4.1. The main reflection of a high signal-to-noise ratio (SNR) reconstructed echo was then used as the clean target signal, and a late-time segment of the same reconstructed record containing diffuse reverberation served as the reverberation component. SRR values from 0 dB to 30 dB in 2 dB steps were obtained by linearly superimposing these two signals and scaling the reverberation amplitude to the desired level. This preserves the measured reverberation characteristics while allowing precise SRR control. Fig. 8 illustrates one example of the construction process, showing the reconstructed target echo, the extracted reverberation segment, and the synthesized mixed echo. Datasets at other SRR levels are generated in the same way.

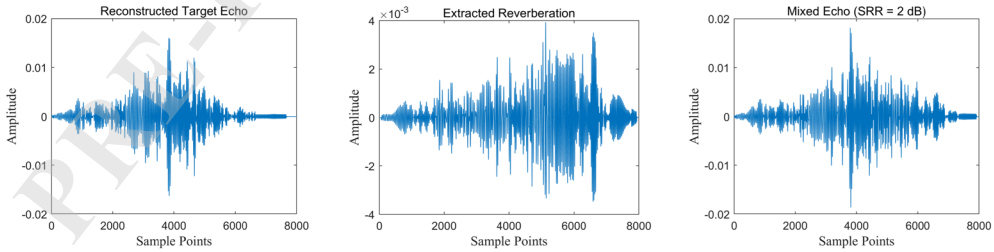

Fig. 8. Waveform Example of a Sonar Mixed Echo (SRR = 2 dB).

Using this method, 16 datasets were constructed with SRRs ranging from 0 dB to 30 dB in 2 dB increments. For each dataset, 50 test samples with known azimuth angles were

uniformly selected from the target's 0°–180° rotation range, with an angular interval of approximately 3.6°. During the similarity matching phase, each test sample was compared with all other samples within the same SRR dataset using a distance-based metric. The sample yielding the minimum cumulative distance was defined as the "optimal matching sample," and the matching error was calculated as the absolute azimuth difference between the two samples. A match was regarded as correct if the azimuth error was less than 10°. This threshold is motivated by the observation that, for the considered target and measurement geometry, the echo characteristics vary only weakly over azimuth intervals of about ±5°, so angular errors within 10° do not lead to perceptible differences in the envelope features used for matching and are acceptable in practical active sonar applications.

The matching accuracy under each SRR condition was defined as the ratio of correctly matched samples to the total number of test samples, serving as a quantitative indicator of the algorithm's robustness to reverberation. Table 1 summarizes the comparative results for AEB-DTW against ED, DTW, and its variants. If two or more methods achieve the same maximum value under a specific SRR condition, each is credited with one win in the overall count. AEB-DTW achieves over 50% accuracy at SRR = 0–2 dB and exceeds 80% when SRR ≥ 24 dB, consistently outperforming all baselines in most conditions.

Table 1. Comparison of Matching Accuracy for Different Algorithms

SRRs	AEB-DTW	DTW	DDTW	WDTW	Sakoe-Chiba	LEDTW	EWDTW	ED	shapeDTW
0	0.54	0.44	0.2	0.54	0.42	0.32	0.36	0.58	0.42
2	0.68	0.4	0.34	0.44	0.42	0.28	0.4	0.52	0.32
4	0.62	0.46	0.4	0.46	0.48	0.34	0.54	0.68	0.46
6	0.7	0.48	0.44	0.54	0.52	0.36	0.44	0.68	0.42
8	0.72	0.46	0.38	0.64	0.52	0.42	0.52	0.7	0.32
10	0.76	0.44	0.36	0.6	0.44	0.36	0.74	0.72	0.46
12	0.74	0.68	0.42	0.72	0.66	0.48	0.7	0.76	0.46

14	0.72	0.74	0.34	0.78	0.80	0.5	0.78	0.8	0.68
16	0.76	0.66	0.42	0.68	0.7	0.4	0.8	0.78	0.66
18	0.8	0.78	0.48	0.78	0.74	0.44	0.86	0.7	0.7
20	0.82	0.7	0.44	0.72	0.66	0.44	0.76	0.78	0.74
22	0.78	0.64	0.4	0.72	0.66	0.5	0.78	0.78	0.7
24	0.84	0.7	0.46	0.82	0.64	0.5	0.78	0.78	0.74
26	0.86	0.64	0.46	0.82	0.6	0.46	0.76	0.8	0.72
28	0.82	0.74	0.48	0.78	0.7	0.46	0.76	0.8	0.72
30	0.84	0.7	0.48	0.8	0.74	0.54	0.76	0.76	0.68
Mean	0.750	0.603	0.406	0.677	0.605	0.425	0.671	0.726	0.575
Wins	11	0	0	0	1	0	3	3	0

To provide a more intuitive comparison of matching accuracy under different SRR conditions, Fig. 9 presents pairwise comparisons between AEB-DTW and ED, DTW, and its variants. Each subplot contains 16 circular markers, representing the matching accuracy under 16 distinct SRR levels. The horizontal and vertical coordinates of each marker correspond to the accuracies of AEB-DTW and the compared algorithm, respectively. Markers on the diagonal line indicate equal accuracy under a given SRR; those below the diagonal indicate that AEB-DTW outperforms the baseline method, while those above indicate that the baseline method achieves higher accuracy than AEB-DTW.

The overall distribution of these points indicates that AEB-DTW tends to deliver superior performance across the tested reverberation conditions. As shown in Fig. 9, it demonstrates higher robustness to reverberation than the other evaluated algorithms.

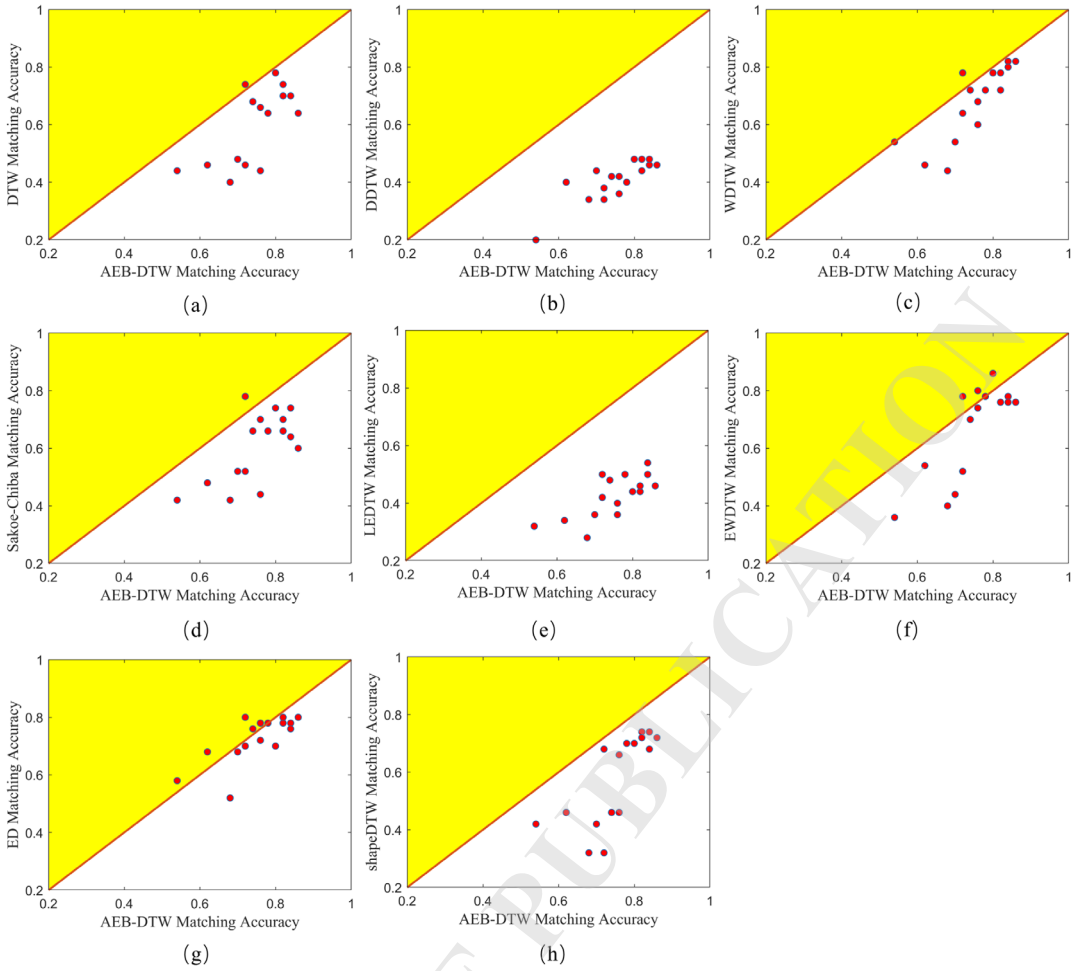

Fig. 9. Matching Accuracy of AEB-DTW vs. ED, DTW, and Its Variants.

4.3 Evaluation of Similarity Measurement Based on Angular Resolution

In active sonar signal recognition, angular resolution measures an algorithm's ability to distinguish echoes from different azimuths. To evaluate this, a dataset with an SRR of 24 dB was used. The 90° echo, representing the median azimuth and exhibiting stable structural features, was selected as the reference. For each algorithm, distances between the reference and other azimuth samples were computed and normalized to the range [0, 1]. The normalized distances were then divided into nine 20° intervals to balance angular granularity and statistical robustness. Within each interval, the mean normalized distance was calculated, and its absolute deviation from 1 was taken as the interval similarity, providing an intuitive measure of signal

discriminability—larger deviations indicate stronger angular separability. Interval-wise similarity profiles for all algorithms are shown in Fig. 10.

DTW shows poor angular resolution due to minimal similarity variation, while DDTW, being insensitive to amplitude, produces abnormally high similarity in low-angle regions. WDTW and Sakoe-Chiba DTW are constrained by fixed weights or rigid boundaries, limiting their performance in high-angle scenarios. ED and EWDTW offer only basic angular discrimination, as ED is restricted to equal-length sequences, and EWDTW relies heavily on hyperparameter tuning. LEDTW and ShapeDTW also exhibit limited sensitivity to angular differences. In contrast, AEB-DTW effectively distinguishes signals with large angular separations while maintaining robustness to local variations. Its adaptive extrema extraction and boundary constraints enable smoother similarity transitions across angles, thereby enhancing angular resolution.

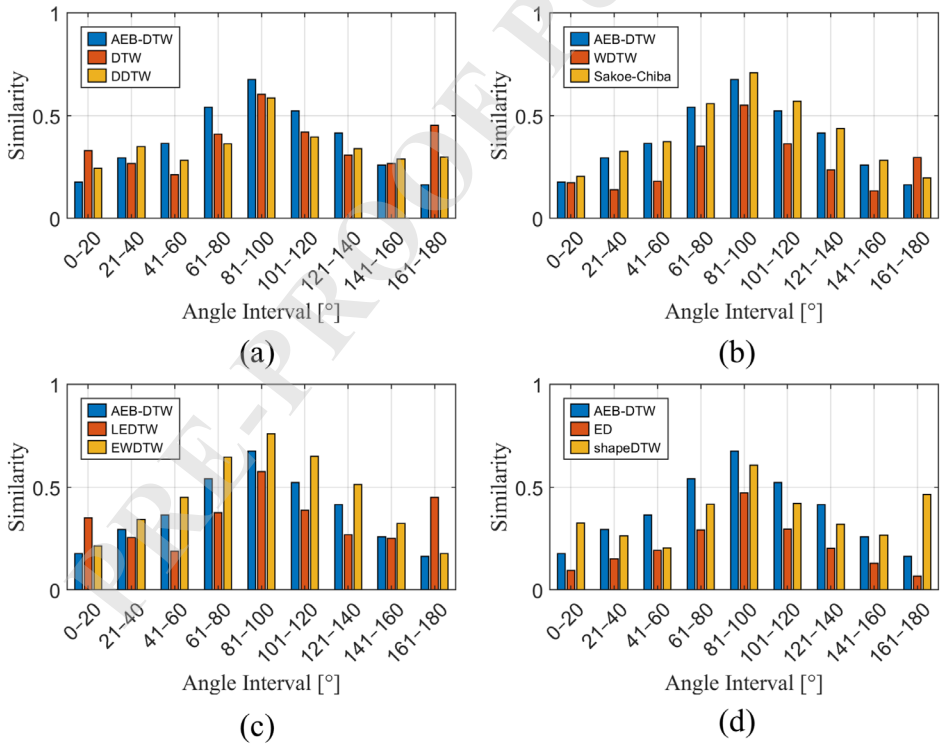

Fig. 10. Angular Resolution Comparison of AEB-DTW and Baseline Methods.

4.4 Comparison of Algorithm Runtime

Fig. 11 shows the comparison of average runtime between AEB-DTW and ED, DTW, and its variants across 16 SRR datasets. Although ED has the shortest runtime, it is only applicable to sequences of equal length and cannot handle asynchronous time axes. LEDTW and EWDTW only account for extrema features without considering structural relationships between extrema, thus lacking global alignment capacity. Among algorithms that support global asynchronous alignment, AEB-DTW demonstrates the best runtime efficiency, verifying its computational advantages.

AEB-DTW shows a clear runtime advantage over other global alignment algorithms, as indicated by its lower average computation time in Fig. 11. Although its runtime is slightly higher than LEDTW and EWDTW, it remains about one order of magnitude lower than DTW and achieves higher matching accuracy (see Table 1), demonstrating a favorable balance between efficiency and accuracy.

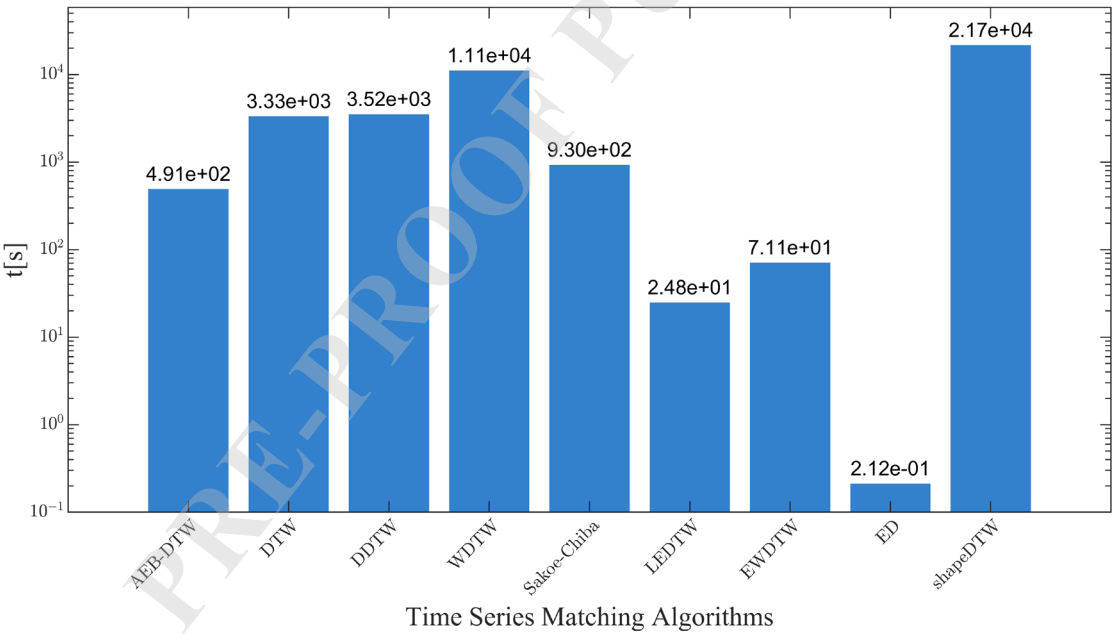

Fig. 11. Average Running Time Comparison.

5 Conclusion

This paper proposes the AEB-DTW algorithm to mitigate the sensitivity of sonar signal

matching to reverberation and the high computational cost of long-duration echoes. The method extracts salient local extrema using an adaptive threshold and aligns them via a joint time–amplitude weighting strategy. Dynamic boundary constraints derived from the extrema alignment path restrict the DTW search region, improving matching efficiency and robustness to structural distortions.

The main findings of the experimental evaluation can be summarized as follows: (1) compared with classical distance-based methods, AEB-DTW achieves higher matching accuracy and stronger robustness to interference; under strong interference conditions with an SRR value of 2 dB, the algorithm still achieves around 70% matching accuracy, demonstrating strong resilience to reverberation; (2) angular-resolution-based similarity evaluation shows that AEB-DTW is more sensitive to azimuth changes and can effectively distinguish echoes originating from different bearing angles, thereby improving the angular discrimination capability of active sonar echo matching; and (3) among algorithms that support global asynchronous alignment, AEB-DTW exhibits the shortest runtime, confirming its significant computational efficiency and indicating that it can reduce computational cost while maintaining high matching performance.

Overall, the algorithm improves both matching accuracy and angular discrimination ability while reducing computational cost, providing an efficient and reliable solution for active sonar echo matching and one-dimensional time-series alignment. Future work will explore multi-target scenarios, nonlinear target motion, variable acoustic environments, and the integration with deep learning methods to further enhance adaptability and recognition performance.

CRediT authorship contribution statement

Tongjing Sun: Data curation, Formal analysis, Investigation, Resources, Writing – review & editing, Funding acquisition, Supervision. **Hunyuan Wang**: Conceptualization, Data curation, Investigation, Methodology, Writing – original draft. **Lei Chen**: Investigation, Methodology, Validation. **Haoran Xu**: Data curation, Formal analysis, Writing – review & editing.

Declaration of Competing Interest

The authors declare that they have no known competing financial interests or personal relationships that could have appeared to influence the work reported in this paper.

Acknowledgment

This article uses experimental data collected at Shanghai Jiaotong University (China), and we gratefully acknowledge our colleagues for their experimental skills. This work was supported by the Joint National Natural Science Foundation of China (No. U22A2044) and the Key Laboratory Fund from Underwater Test and Control Technology (No. 2023-JCJQ-LB-030).

References

[1] Bian J.C., Xue S.Q., Zhao S., Xiao Z., Gao J.L. (2024), Analysis of sonar window navigation accuracy under different seabed beacon configurations, *Navigation and Control*, **23**(Z1): 78–83, https://doi.org/10.11993/j.issn.2096-3920.2017.01.002.

[2] Chen H.Y., Liu C.H., Sun B. (2017), Survey on similarity measurement of time series data mining, *Control and Decision*, **32**(1): 1–11, doi: 10.13195/j.kzyjc.2016.0462.

[3] Dau H.A., et al. (2018), Optimizing dynamic time warping's window width for time series data mining applications, *Data Mining and Knowledge Discovery*, **32**: 1074–1120, https://doi.org/10.1371/journal.pone.0036556.

[4] Hong J.Y., Park S.H., Baek J.G. (2020), SSDTW: Shape segment dynamic time warping, *Expert Systems with Applications*, **150**: 113291, https://doi.org/10.1016/j.eswa.2020.113291.

[5] Jeong Y.S., Jeong M.K., Omitaomu O.A. (2011), Weighted dynamic time warping for time

series classification, *Pattern Recognition*, **44**(9): 2231–2240, https://doi.org/10.1016/j.patcog.2010.09.022.

[6] Keogh E., Ratanamahatana C.A. (2005), Exact indexing of dynamic time warping, *Knowledge and Information Systems*, **7**: 358–386, doi: 10.1007/s10115-004-0154-9.

[7] Keogh E.J., Pazzani M.J. (2001), Derivative dynamic time warping, [In:] *Proceedings of the 2001 SIAM International Conference on Data Mining*, pp.1-11, SIAM, https://doi.org/10.1137/1.9781611972719.1.

[8] Kim S.W., Park S., Chu W.W. (2001), An index-based approach for similarity search supporting time warping in large sequence databases, [In:] *Proceedings 17th International Conference on Data Engineering*, pp. 607–614, Heidelberg, https://doi.org/10.1109/ICDE.2001.914875.

[9] Lahreche A., Boucheham B. (2021), A fast and accurate similarity measure for long time series classification based on local extrema and dynamic time warping, *Expert Systems with Applications*, **168**: 114374, https://doi.org/10.1016/j.eswa.2020.114374.

[10] Li H. (2021), Time works well: Dynamic time warping based on time weighting for time series data mining, *Information Sciences*, **547**: 592–608, https://doi.org/10.1016/j.ins.2020.08.089.

[11] Li H.H., Liu J.X., Yang Z.L, Liu R.W., Wu K.F., Wang Y. (2020), Adaptively constrained dynamic time warping for time series classification and clustering, *Information Sciences*, **534**: 97–116, https://doi.org/10.1016/j.ins.2020.04.009.

[12] Li H.L., Guo C.H. (2013), A review of research on feature representation and similarity measurement in time series data mining, *Computer Application Research*, **30**(5): 1285-1291, doi: 10.3969/j.issn.1001-3695.2013.05.002.

[13] Sakoe H., Chiba S. (1978), Dynamic programming algorithm optimization for spoken word recognition, *IEEE Transactions on Acoustics, Speech, and Signal Processing,* **26**(1): 43–49, doi: 10.1109/TASSP.1978.1163055.

[14] Salvador S., Chan P. (2007), Toward accurate dynamic time warping in linear time and space, *Intelligent Data Analysis*, **11**(5): 561–580, https://doi.org/10.3233/IDA-2007-11508.

[15] Silva D.F., Giusti R., Keogh E., Batista G.E.A.P.A. (2018), Speeding up similarity search under dynamic time warping by pruning unpromising alignments, *Data Mining and Knowledge Discovery*, **32**: 988–1016, https://doi.org/10.1007/s10618-018-0557-y.

[16] Sun S., Qiu J.X., Liu Z., Wang J.Y., Wang J.H. (2024), A method for sonar pulse matching recognition based on time-frequency matrix, *Journal of Electroacoustics*, **48**(11): 64–69, https://doi.org/10.16311/j.audioe.2024.11.020.

[17] Tang W.F., Gao C.F. (2023), Dynamic time warping algorithm with adaptive weighting of extreme points, *Computer Engineering*, **49**(7): 150–160, https://doi.org/10.19678/j.issn.1000-3428.0065500.

[18] Wang C., Long Y.W., Yin W.H., Huang B. (2022), Research on distance measurement method based on improved DTW lower bound function, *Computer Engineering and Applications*, **58**(23): 316–326, doi: 10.3778/j.issn.1002-8331.2106-0036.

[19] Yi B.K., Jagadish H.V., Faloutsos C. (1998), Efficient retrieval of similar time sequences under time warping. [In:] *Proceedings 14th International Conference on Data Engineering*, pp. 201–208, Orlando, https://doi.org/10.1109/ICDE.1998.655778.

[20] Zhang M.Y., Cai W.Y., Wang Y.H., Zhu J.F. (2023), A level set method with heterogeneity filter for side-scan sonar image segmentation, *IEEE Sensors Journal*, **24**(1): 584–595, https://doi.org/10.1109/JSEN.2023.3334765.

[21] Zhao J.P., Itti L. (2018), shapeDTW: Shape dynamic time warping, *Pattern Recognition*, **74**: 171–184, https://doi.org/10.1016/j.patcog.2017.09.020.

[22] Zhu Z.R., Tao C.H., Wu T., J. Schneider von Dämeling., Zhang J.H., Zhang G.Y. (2025), Seafloor classification by fusing AUV acoustic and magnetic data: towards complex deep-sea environments, *IEEE Transactions on Geoscience and Remote Sensing*, **63**: 1-15, https://doi.org/10.1109/TGRS.2025.3545128.